JOURNAL OF CATALYSIS 96, 326–346 (1985)

Nonlinear Kinetics in Catalytic Oxidation Reactions: Periodic and Aperiodic Behavior and Structure Sensitivity

M. SHEINTUCH

Department of Chemical Engineering, Technion-Israel Institute of Technology, Haifa 32000, Israel

Received April 4, 1984

A general mechanism of nonlinear kinetic steps is suggested to account for kinetic instabilities in catalytic oxidation reactions and several isothermal oscillatory models are derived from it. There is still insufficient experimental evidence to construct a detailed model. Physicochemical considerations suggest, however, that the simplest, yet realistic, model should incorporate two surface concentrations as dynamic variables and a slow surface modification such as an oxidation and reduction step. Analysis of the ability of each model to provide efficient communication across the surface shows that the incorporation of thermal and gas-phase concentrations effects is necessary to assure synchronized oscillations. Periodic behavior may emerge in a nonisothermal system with autocatalytic kinetics when its heat capacity is sufficiently large. Coupling of thermal and surface modification effects can lead to complex behavior in the form of multipeak or chaotic oscillations. Periodic behavior can be attributed also to a mechanism incorporating a homogeneous branching and heterogeneous generation steps of a reaction intermediate. Nonlinear kinetics and structure sensitivity are common to oxidation reactions, suggesting a possible relation between these phenomena. Size-dependent kinetics may emerge due to symmetry breaking of the state of a system when surface communication is poor. Apparent structure sensitivity may be observed when a heterogeneous–homogeneous mechanism applies and the active area to catalyst volume ratio is not maintained constant.

INTRODUCTION

Sustained oscillatory behavior has been observed in a large number of oxidation reactions catalyzed by transition metals of Groups VIII and IB (Fig. 1). This behavior was documented for platinum-catalyzed oxidation of carbon monoxide (*1*), hydrogen (*2*), ammonia (*3*), ethylene (*4*), propylene (*3*), and other fuels. Cross-catalyst studies were conducted for CO oxidation (Pt, Pd, Ir (*6*), and Cu), H_2 oxidation (Pt, Pd, Ni (*2, 7*)), and their mixture in city gas (Co, Ni, Cu (*8*)). Oscillations with noble-metal catalysts were usually observed with large oxygen-to-fuel ratio while studies with Co, Ni, or Cu catalysts employed stoichiometric or fuel-rich mixtures. Oscillations during CO oxidation on Pt were observed with a variety of catalyst configurations (in the form of a wire, a foil, or supported on a pellet) immersed in a CSTR or in a stream of premixed reactants.

A necessary condition for the occurrence of oscillatory behavior is the existence of an autocatalytic step where a species inhibits the rate of its reaction or accelerates the rate of its production. We will refer to this species concentration as the autocatalytic variable. Such steps are common in oxidation reactions where reactant inhibition due to competitive chemisorption is evident from negative order kinetics. Another necessary condition for periodic behavior is the coupling between two or more variables. Thus, at least two rate-determining steps are required to account for oscillations in an isothermal system, of which one rate should exhibit a nonmonotonic behavior.

Although a large number of mathematical models have been suggested in the litera-

0021-9517/85 $3.00

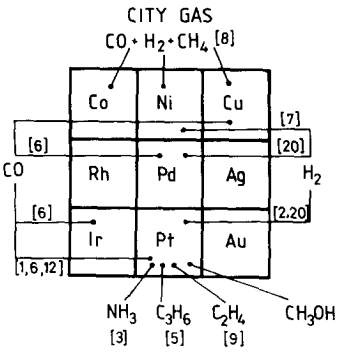

FIG. 1. Observations of periodic and aperiodic behavior in catalytic oxidation reactions catalyzed by transition metals (partial list of references is shown).

ture, there is no agreement yet on the chemical source of the behavior or whether all the observations of catalytic oscillations are of the same origin. Measurement of reaction rate and surface potential during H_2 oxidation on Ni (*7*) demonstrated that the surface undergoes a cyclic process of oxidation and reduction during the oscillations. Strong evidence for the applicability of this mechanism in Pt-catalyzed reactions have been documented in ethylene (*4*) and CO (*6*) oxidation. In the former case Vayenas *et al.* employed solid electrolyte potentiometry to show that the boundary of oscillatory behavior is similar to the thermodynamic stability limit of Pt oxide (*9*). In the latter case Sales *et al.* (*10*) showed that the time scales of surface oxidation and reduction are similar to the oscillations periods. Riekert (*11*) used thermodynamic arguments to show that in the temperatures and concentrations range where periodic behavior was observed, both the metal and its oxide are stable and this transition can account for the observed behavior on Ni, Pd, and Pt. In CO oxidation on Pt, several studies have observed the onset of periodic behavior after the introduction of small amounts of impurities (*12*). Recent investigations, however, have observed periodic behavior even under conditions of high purity of the feed and the metal (*6*).

The next chapter summarizes some of the suggested mechanisms into classes that differ in the nature of the dynamic variables (gas-phase or surface concentration) and emphasize the importance of understanding the nature of the autocatalytic steps and variables. The other variable may differ in nature. The variety of possible nonautocatalytic steps may render the observation of periodic behavior difficult for reproducibility and that may be the source of some of the contradicting observations reported in the literature.

A natural source for autocatalysis in the highly exothermic and highly activated oxidation reactions is acceleration due to temperature effects. The thermokinetic mechanism, however, was ruled out by most researchers due to (a) observations of oscillations in isothermal systems, (b) theoretical considerations showing that the large heat capacity of the solid would stabilize the system, and (c) the observation that in most cases the period of the oscillations (10–1000 s) is much larger than the characteristic time scale of the reaction, taken to be the inverse turnover number (1–10 s^{-1}). A thermokinetic model will predict fast oscillations with a period that is of the order of magnitude of the inverse turnover number or shorter. The existence of two widely different time scales simplifies the stability analysis and analytical solution of the nonlinear model is then possible. The period of the oscillations is of order of magnitude of the slow process.

In the third chapter we show that periodic behavior may emanate from the coupling of mass and heat balances if the temperature assumes the role of the nonautocatalytic variable, thus still requiring the existence of an autocatalytic kinetic step. Periodic behavior can be then simulated with arbitrarily small temperature fluctuations when the heat capacity is sufficiently *large*. If such a model is coupled with a third kinetic balance for some surface modification, in a way that temperature plays the role of the nonautocatalytic variable with respect to the main reaction

while it is autocatalytic variable with respect to the slow surface modification, then such a model may predict multipeak oscillations and chaotic (i.e., time-dependent aperiodic) behavior. Nonisothermal models for chaotic behavior have been suggested before (*13*), yet without demonstrating the systematic approach for constructing the model. A similar approach, made possible by the existence of three widely-separated time scales, has been employed by Chang and Aluko (*14*) in the analysis of a purely kinetic model. The topology in Ref. (*14*) is different from the one analyzed here.

Apparently, there exists some form of communication within the catalyst to assure the synchronization of the periodic behavior. In the lack of such synchronization the system will exhibit a time-invariant average rate of the randomly phased oscillators. In the fourth section we consider the ability of each model to provide efficient communication. This problem, i.e., the dynamics of reaction-diffusion equations, was considered by Pismen (*15*) and was applied to catalytic surfaces by Sheintuch and Pisemen (*16*). To convey the physical arguments involved, we consider here an approximation to the continuous problem in the form of two identical cells exchanging heat and mass with the surroundings as well as between themselves. This configuration may represent two interacting pellets in a CSTR, two communicating crystallites within a pellet or protrusions within a wire, or even two faces of the same crystallites. Each situation is characterized by a typical length scale, and we consider the ability of each model to assure synchronization over these scales. This ability is strongly dependent on the diffusivity of the autocatalytic variable, and can be used as a consideration in the process of discrimination among the models.

The uniform solution, which is always a mathematical solution to the homogeneously exposed catalyst, may become unstable under conditions of poor communication and a new asymmetric state arises. This was demonstrated for the two-cells problem by Prigogine and Lefever (*17*) and by Pismen (*18*) for the continuous problem. The existence of asymmetry and the average reaction rate in that state are crucially dependent on the size of the system. Thus, there may exist a possible connection between nonlinear kinetics and structure sensitivity, the dependence of reaction rate per unit surface area on crystalline size. Such a dependence was simulated by the author (*19*) by studying the size-dependent behavior of a continuous one-dimensional single crystallite having a uniform activity of all its sites. These results are compared here with experimental observations of structure sensitivity. This origin of the phenomenon is conceptually different from the usual approach which attributes the phenomenon to nonuniform activity of edge vs bulk sites. The possible connection between oscillatory behavior and structure sensitivity is based on the observation that both are common to oxidation reactions and were observed under similar conditions during the studies of H_2 oxidation on Pd (*20*) and CO oxidation on Pt (*1*).

The last chapter considers the idea of a heterogeneous–homogeneous reaction as a source for oscillatory behavior and structure sensitivity. In that mechanism we incorporate a branching autocatalytic step of an intermediate gas-phase species that is initiated and terminated on the surface. This autocatalytic step is the one responsible for the cool-flame oscillations in homogeneous oxidation reactions. There is strong evidence for the importance of heterogeneous–homogeneous mechanisms in olefin and other hydrocarbon oxidation with stoichiometric or fuel-rich mixtures (*21*). Homogeneous reaction is believed to be negligible at low temperatures, and fuel concentrations below the explosion limit. These are conditions that were employed in most observations of catalytic oscillations. Several studies of catalytic reactions suggested, however, that this step may not be neglected at temperatures as low as 100°C

with several mol percents of H_2, CO (*22*), or C_2H_6 (*23*). In a study of oscillations during Pt-catalyzed ammonia oxidation (30% in air) the existence of a homogeneous reaction was visually observed in the form of a flame propagating from the wire in the upstream direction (*3*). This suggests that at lower temperatures and concentrations the homogeneous reaction may be confined to the boundary layer and escapes visual observation. Ostapiuk *et al.* (*22*) have employed differential calorimetry to conclude that steady-state multiplicity and oscillations in CO oxidation on Pd are induced by heterogeneous–homogeneous mechanisms. A heterogeneous–homogeneous mechanism was suggested by Berman and Elinek (*24*) to account for oscillations in cyclohexane oxidation on a zeolite catalyst. The mechanism suggested here incorporates the basic necessary steps and extends the analysis to account for apparent structure sensitivity when the active surface area per unit volume of catalyst is varied during the experiment.

NOMENCLATURE

A_v	active surface area per unit volume
a_v	intercell exchange area per unit volume
C_1, C_2	fuel and oxygen concentrations in the gas phase
c	dimensionless concentration
D	diffusivities
d, e	functions
E	activation energy
F	fuel species
f, g	dimensionless kinetic functions
H, h	dimensionless and dimensional heat transfer coefficient
I	intermediate species
k_e	exchange coefficient
k_i	rate constants
K_1, K_2	adsorption coefficients of fuel and oxygen
L_i	characteristic length scales
l	spatial coordinate
M_a	mass capacity of adsorbed phase
mC_p	catalyst heat capacity
M_i	capacity of phase i
P	poisonous species
r	reaction rate
s, s^*	reduced and oxidized site, respectively
S_g	total surface area per unit volume
S_x	external catalyst area per unit volume
T	temperature
t	time
x, y, z	dimensionless dynamic variables
Y	temperature dependence defined in Eq. (6).

Greek Letters

α, β, γ	dimensionless kinetic parameters
ΔH	heat of reaction
τ_i	characteristic time scales
$\theta_1\theta_2$, θ_p, θ^*	fractional surface coverages of fuel, oxygen, poison, and oxidized surface, respectively
Γ_i, Γ_e	projection of the ignition and extinction lines

Subscripts

a	of adsorption step
b	at bulk conditions
d	of desorption step
r	of surface reaction step
s	in adsorbed state
x, y	of x or y

ISOTHERMAL OSCILLATORY KINETICS

(*a*) *Physical Consideration*

The general model for catalytic kinetics usually assumes the existence of several phases (Fig. 2) which may or may not be in instantaneous equilibrium. The bulk phase equations account for flow of mass and enthalpy and their transport to the surface.

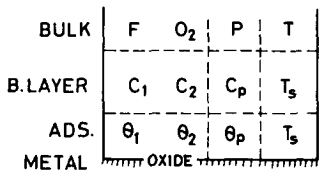

FIG. 2. Various phases and dynamic variables employed in modeling of catalytic kinetics.

Diffusion and adsorption take place in the boundary layer, which may represent the pore volume in a porous catalyst or the stagnant boundary layer around a wire. The adsorbate phase equations incorporate the processes of adsorption, reaction, and surface modification and its dynamic variables are surface concentrations. Modification in the form of surface oxidation and reduction requires the incorporation of the metal phase into the model. Within each phase we have to account for concentrations of reactants and products (when desorption is not instantaneous). Other variables to be included are poison concentration whenever it affects the rate and surface temperature when thermal effects are not negligible.

The general scheme is too complex for investigation and the modeling process focuses therefore on determining the most simple, yet realistic, set of dynamic variables to account for periodic behavior.

Justification for eliminating some of the variables is based on physical grounds; e.g., in a flow situation past a wire or a pellet the bulk conditions may be assumed constant, and when the reaction is sufficiently slow then gradients across the boundary layer may be negligible. The model accounts then only for purely catalytic steps. Such a situation may be achieved at low pressures; in all noble-metal-catalyzed CO oxidation studies thermal and mass transport resistances have not been eliminated under atmospheric pressure. In these studies the importance of the coupling between physical and kinetic steps, for the generation of periodic solutions, has to be settled on purely theoretical considerations. Further elimination of variables requires the postulation of certain assumptions concerning adsorption equilibrium of the fuel and/or oxygen and the importance of poisoning, surface oxidation, or any other modification of the surface.

By employing this set of assumptions the general model can be reduced to a two-variable problem. The theoretical investigation proceeds then to find the simplest steps that admit periodic solutions. The logical candidate for the autocatalytic step in isothermal models is the reaction step. The simplest molecularity of that step depends then on the adsorption kinetics, whether dissociative or not, as was shown by Sheintuch and Schmitz (*25*). Trimolecular steps are necessary to produce oscillations in a two-variable model with polynomials rate expressions (*26*). Bimolecular steps, however, may be sufficient in a three-variable model (*10*). Thus, the details of the kinetics can be tuned to the set of assumptions and the selected dynamic variables. In the following discussion we choose the simplest possible mathematical steps.

Almost any combination of two variables will admit periodic solutions when the proper assumptions, kinetic and/or thermal effects, are incorporated into the model. Such an analysis cannot reveal the chemical origin of the phenomena but may identify the phases of the autocatalytic and non-autocatalytic variables. We emphasize the importance of the proper choice of the two variables. The phases differ in their capacity for mass or heat, and in the corresponding diffusivities which determine the degree of communication and synchronization across the surface. Note that both characteristics do not affect the steady-state value but determine its stability. We delay the investigation of the communication effect to a later section and proceed with a study of lumped (i.e., space independent) parameter systems.

(*b*) *The Kinetic Scheme* (*Table 1*)

The general kinetic scheme of $F + O_2 \rightarrow$ B accounts for adsorption of F (fuel) and O_2

TABLE 1

General Kinetic Scheme for $F + O_2 \rightarrow B$

	Transport		Surface oxidation	
(T)	$F(\text{bulk}) \rightarrow F(\text{reactor})$	$r_T = k_T(C_{1b} - C_1)$	$O_{2s} \rightarrow s^*$	
	Adsorption		(5) or $O_{2s} + s \rightarrow 2s^*$	$r_5 = k_5\theta_2^{\mu}\theta_v'^2$
(1)	$F + s \rightleftarrows F_s$	$r_1 \equiv k_{1a}C_1\theta_v - k_{1d}\theta_1$	Surface reduction	
(1E)	$F + s \rightleftarrows F_s$	$\theta_1 \equiv K_1C_1(\theta_v + \theta_1)/(1 + K_1C_1)$	Step 4	
(2)	$O_2 + s \rightleftarrows O_{2s}$	$r_2 \equiv k_{2a}C_2\theta_v - k_{2d}\theta_2$	(6) $F^* + s^* \rightarrow B + s$	$r_6 \equiv k_6C_1\theta^*$
(2E)	$O_2 + s \rightleftarrows O_{2s}$	$\theta_2 \equiv K_2C_2(\theta_v + \theta_2)/(1 + K_2C_2)$	Surface poisoning	
	Main reaction		(7) $P + s \rightleftarrows P_s$	$r_7 \equiv k_{7a}\theta_v - k_{7d}\theta_p$
(3)	$\mu F_s + O_{2s} \rightarrow B + (\mu + 1)s$	$r_3 \equiv k_3\theta_2\theta_1^{\mu}$ $\mu = 1$ or 2		
(4)	$\mu F_s + s^* \rightarrow B + 3s$	$r_4 \equiv k_4\theta^*\theta_1^{\mu}$		

(steps 1, 2), which may or may not be in equilibrium. Nondissociative adsorption is assumed for the sake of simplicity and generality. Allowing for dissociation of F and/or O_2 upon adsorption would not alter the results. Surface reaction between chemisorbed fuel and adjacent adsorbed oxygen (step 3, a Langmuir–Hinshelwood mechanism) or adjacent oxidized site (step 4) may be a bi- or trimolecular step. Surface oxide is formed by adsorbed oxygen (step 5) or may occur at a rate proportional to the main reaction (not shown here, see (*16*)). Surface reduction, aside from being the main reaction, may occur at a slow rate by F adsorbed on the oxide (F^* in equilibrium with the gas phase, step 6) so as to avoid complete irreversible oxidation of the surface. Surface poisoning is assumed to involve a linear adsorption and desorption steps (step 7). Other surface modifications can be also incorporated.

(*c*) *Analysis of Motion*

The large difference between the turnover number and the oscillation frequency suggests the existence of two time scales. A necessary condition for the existence of oscillations then is that the autocatalytic variable (denoted by x) can acquire multiple solutions for a certain range of the nonautocatalytic one (y). This condition poses certain restrictions on the order of the autocatalytic reaction while the accurate kinetics of the other steps is of secondary importance. When chemisorption equilibrium is assumed (Model I, Table 2) then a bimolecular Langmuir–Hishelwood reaction rate acquires a local maximum with respect to C_1. The fuel gas-phase concentration is chosen as autocatalytic variable. The actual rate curve is dependent on the modified fraction of surface which, for the sake of simplicity, is assumed to be inactive due to poisoning or oxidation. Coupled with a linear flow term (dotted line, Fig. 3a) there are three solutions of x for $y = y_2$, while only one for y_1 or y_3. The steady state of the system, which can be described by

TABLE 2

Oscillatory Models

Model	Autocatalytic set				Nonautocatalytic set			Necessary conditions	Synchronization	Ref.
	Var.	Steps	Equations and assumptions	L_x (cm)	Var.	Steps	L_y (cm)			
I	F $x = C_i/C_b$	T, 1E, 2E, $3(\mu = 1)$	$1 - x - \alpha x\left(\frac{1-y}{1+K_iC_bx}\right)^2$ $\theta_2 \ll 1$	1	$s^*, y = \theta^*$	5, 6	10^{-4}	$K_iC_{ib} > 8$	Good on a pellet scale or lower	*16* *16*
					$P_s, y = \theta_p$	7	10^{-2}			
II	s^* $x = \theta^*$	1E, 2E, $4(\mu = 2)$ $5(\nu_1 = 1 - \nu_2 = 0)$, 6	$1 - x - \alpha y^2(1-x)^2x - \beta x$ $K_iC_i \ll 1$	10^{-5}–10^{-6}	F $y = C_i/C_{ib}$	T, 4, 6 $\mu = 2$	10	$8\beta < 1$	Symmetry breaking	*19*
III	O_{2s} $x = \theta_2$	1E, 2, $3(\mu = 2)$	$1 - x - y - \alpha(1-x-y)^2x - \beta x$	10^{-2}–10^{-3}	$s^*, y = \theta^*$	5, 6	10^{-4}	$\alpha > 1 > 8\beta$	Poor in a pellet, local osc. in unsupported cat., bulk osc. disappear in large systems	*16* *27*
					$P_s, y = \theta_p$	7	10^{-2}			
IV	F_s, O_{2s} $x_{1,2} = \theta_{1,2}$	1, 2(dis.), $3(\mu = 1)$	$g_1 = \theta_v - \beta x_1 - \gamma x_1x_2$ $g_2 = \alpha\theta_v^2 - \gamma x_1x_2$ $\theta_v = 1 - x_1 - x_2 - y$	10^{-2} – 10^{-3}	s^* $y = \theta^*$	4,5 $\mu = 1$	10^{-4}	Not given		*10*
V	s^* $x = \theta^*$	1E, 2E, $4(\mu = 2)$ $5(\nu_1 = 1 - \nu_2 = 0)$, 6	$1 - x - y - \alpha c^2x(1-x-y)^2 - \beta cx$ $K_iC_i \ll 1$	10^{-5}–10^{-6}	P_s $y = \theta_p$	7	10^{-2}	$8\beta c < 1$	Structure sensitivity	*19*

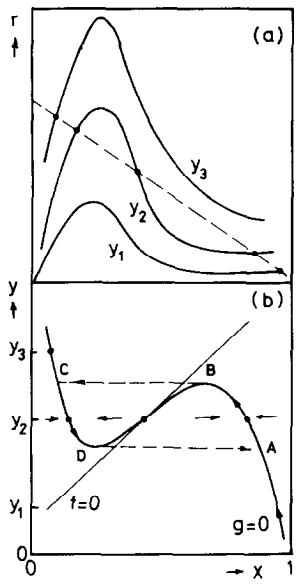

FIG. 3. Graphical construction of oscillatory solutions when a wide separation of time scales exists.

$$\tau_x \frac{dx}{dt} = g(x, y)$$

$$\tau_y \frac{dy}{dt} = f(x, y), \qquad (1)$$

is the intersection of $g(x, y) = 0$ which is multivalued (Fig. 3b) and $f(x, y) = 0$. Coupling between the two variables can lead to oscillatory behavior if they compete for adsorption sites in such a way that a unique steady state exists on the intermediate branch of $g(x, y) = 0$ (say, at y_2). Now τ_x, τ_y are the time scales of the two variables (Eq. (1)) and f, g are scaled to be of order one. When the gas-phase concentration responds much faster to perturbation than the surface modification ($\tau_x/\tau_y \ll 1$), then

$$\frac{dx}{dy} = \frac{\tau_y}{\tau_x} \frac{g(x, y)}{f(x, y)} \to \infty. \qquad (2)$$

Thus, the motion in the phase plane (x vs y) is horizontal and fast everywhere except close to $g = 0$ where the nonautocatalytic function is controlling the velocity. To assure bounded solutions the direction of motion is as shown in Fig. 3b. It is clear that the unique state is unstable and is surrounded therefore by a limit cycle. Along that cycle (ABCD) the system follows the two stable branches of $g(x, y) = 0$ and then jumps, with a time scale of τ_x, from one branch to another.

The identity and the kinetic form of the surface modification are of secondary importance and $f(x, y)$ may be taken to be linear. The oscillations are of period τ_y in order of magnitude and that may provide a clue to the identity of the nonautocatalytic variables (*10*). The time scales are the ratios of the respective phase capacity to characteristic reaction velocity, $\tau_i = M_i/k$. The ratio of mass capacities of the gas to the solid phase[1] is large in a CSTR (*16*), around unity in a flow past a wire, and very small in a porous particle. To assure wide separation of time scales, in a CSTR or a wire, surface modification should be made sufficiently slow in comparison with the reaction.

(d) Other Oscillatory Models

The gas-phase concentration can be made to be the nonautocatalytic variable when the main reaction proceeds via surface oxidation and reduction; the oxide concentration plays then the role of the autocatalytic one (Model II). Now, since both variables vary at similar rates of r_4, separation of time scales can be achieved when the capacity of the gas phase is much larger than that of the chemisorbed phase. Such a model applies, therefore, to a CSTR or a wire but may not admit periodic solutions when a pellet is considered.

When both variables are of similar capacities then one rate-determining step, say surface modification, should be much slower than the main reaction in order to achieve different time scales. Since both fuel and oxygen participate in the main reaction, any model that has C_1 and C_2 or θ_1

[1] This ratio is $\delta C_b/M_a$ where δ is the boundary layer thickness and M_a is the adsorption capacity ($\sim 2 \times 10^{-9}$ mol/cm^2). For C_b of 1 vol% $C_b/M_a \sim 100$ cm^{-1}.

and θ_2 for variables cannot achieve timescales separation. The only possible combination of variables left for investigation is that of a chemisorbed reactant concentration and a fraction of modified surface. In Model III x is adsorbed oxygen and y is the surface oxide or a poisonous species and we assume that the system is free of any physical resistances. Another possible oscillator is that of an autocatalytic surface oxidation and reduction coupled with a slow poisoning (Model V). Sales *et al.* (*10*) considered an oscillator with three variables: the two adsorbed reactant concentrations are the fast variables while surface oxidation and reduction is the slow process (Model IV). Fuel adsorption is assumed to be linear, oxygen adsorption is dissociative (unlike in step 2) and irreversible, and surface reaction proceeds via a bimolecular step. The motion of the system

$$\tau_x \frac{dx_1}{dt} = g_1(x_1, x_2, y),$$

$$\tau_x \frac{dx_2}{dt} = g_2(x_1, x_2, y),$$

$$\tau_y \frac{dy}{dt} = f(x_1, x_2, y) \qquad (3)$$

when $\tau_x/\tau_y \ll 1$ is similar to that of Eq. (1): slow along the stable sections of $g_1 = g_2 = 0$, which form a line in the (x_1, x_2, y) space, and fast at constant y elsewhere. Thus, we can analyze the system by examining its projection to the (x_1, y) or (x_2, y) plane. The assumption of dissociative oxygen adsorption is necessary to render the projection of $g_1 = g_2 = 0$ multivalued when the reaction is bimolecular.

The observations of oscillations in a variety of experimental setups, varying in their flow patterns and the ratio of fluid-to-solid phase capacities, suggest that mass transfer resistances are not crucial for the existence of oscillations. That conclusion is supported by observations, made in H_2 oxidation on Ni (*7*) and Pd showing that when the linear velocity is increased significantly, the oscillation persists and the characteristics of this behavior (bifurcation points, periods, average rate) reach asymptotic values. In several other systems, notably CO oxidation on Pt, mass and heat transfer resistances could not be eliminated under atmospheric conditions. Oscillations in this reaction were detected, however, at low pressures (10^{-4} Torr (*28*)) under conditions where transport resistances are negligible.

THERMAL EFFECTS AND COMPLEX BEHAVIOR

(a) *The Model*

The arguments against the thermokinetic mechanism as a source of periodic behavior have already been outlined in the Introduction. Since transport effects are not crucial for the existence of periodic behavior, let us consider thermal effects associated with Model III. The equations describing the system

$$M_a \frac{d\theta_2}{dt} = r_a - r_r; \qquad M_a \frac{d\theta^*}{dt} = r_{oxi} - r_{red}$$

$$mC_p \frac{dT}{dt} = h(T_b - T) + (-\Delta H_a)r_a + (-\Delta H_r)r_r$$

$$r_a = k^\circ_{2a} C_{2b} e^{-E_a/RT}\theta_v - k^\circ_{2d} e^{-E_d/RT}\theta_2$$

$$r_r = k^\circ_3 e^{-E_3/RT}\left(\frac{K_1C_1}{1 + K_1C_1}\right)^2 (\theta_v + \theta_1)^2 \cdot \theta_2 \qquad (4)$$

account for adsorption and reaction of oxygen and their thermal effects and the slow process of surface oxidation and reduction. The enthalpy contribution of the latter was ignored and the heat transfer resistance is expressed in the usual linear form.

We have already shown that the isothermal version of Eq . (4) admits periodic solutions. We intend to show now that such behavior exists even when surface modification is ignored and that incorporating both effects may result in chaos (aperiodicity). Thus, for the sake of demonstration and in order to deal with as few parameters as possible, assume that $\theta_1 \ll \theta_v$ (i.e., K_1C_1

$\ll 1$ and $\theta_v = 1 - \theta_2 - \theta^*$) and that $-\Delta H_a = 0$ (i.e., $E_a = E_d$). Defining the variables as

$$x = \theta_2,$$
$$y = \frac{(E_a - E_3)}{RT_b}\left(\frac{T - T_b}{T_b}\right),$$
$$z = \theta^*. \tag{5}$$

We rewrite the system in the form

$$\tau_x \frac{dx}{dt} = Y^n\left[1 - x - z - \beta x - \frac{c^2}{Y}x(1 - x - z)^2\right] \equiv g(x, y, z)$$
$$\tau_y \frac{dy}{dt} = -Hy + c^2 Y^{n-1} x(1 - x - z)^2 \equiv f(x, y, z)$$
$$\tau_z \frac{dz}{dt} = h(x, y, z)$$
$$Y = \exp\left(\frac{y}{1 + y/\gamma}\right), \tag{6}$$

where the parameters are defined as

$$\gamma = \frac{E_a - E_3}{RT_b},$$
$$n = \frac{E_a}{E_a - E_3},$$
$$c^2 = \frac{k_3 K_1^2 C_1^2}{k_{2a} C_{2b}},$$
$$H = \frac{hT_b}{\gamma(-\Delta H_r)k_{2a}C_{2b}},$$
$$k_{2a} = k_{2a}^\circ \exp(-E_a/RT_b), \tag{7}$$

where c^2 is the dimensionless fuel concentration and H is the dimensionless heat transfer coefficient. The time scales are

$$\tau_x = \frac{M_a}{k_{2a}C_{2b}},$$
$$\tau_y = \frac{mC_pT_b}{(-\Delta H_r)\gamma k_{2a}C_{2b}},$$
$$\tau_z = \frac{M_a}{k_{oxi}}. \tag{8}$$

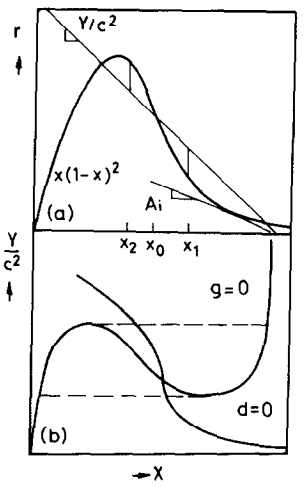

FIG. 4. Graphical construction of oscillatory solution for nonisothermal catalyst with large heat capacity.

(b) *Simple Periodicity in Nonisothermal Systems*

Both x or y can play the role of the autocatalytic variable. Let us ignore, for the moment, the effect of surface modification (i.e., $z = 0$). The $g = 0$ curve is obtained from the intersection of $x(1 - x)^2$ with the straight line $(1 - x - \beta x)Y/c^2$ (Eq. (6)) by varying the slope of the latter (Fig. 4a). When $8\beta < 1$ the resulting curve is multivalued when plotted in the (Y, x) phase plane (Fig. 4b). Since there is a one-to-one correspondence between y and Y we may choose the latter as an ordinate. This model will admit therefore periodic solutions when there exists a unique steady state on the middle branch of $g = 0$ and $\tau_x \ll \tau_y$. The latter requirement clearly implies that the catalyst heat capacity should be sufficiently *large* while the former is satisfied when $E_a > E_3$ ($\gamma > 0$). To prove this, combine $f = 0$ with $g = 0$ from Eq. (6) to find

$$d(x, y) \equiv Y^n(1 - x - \beta x) - Hy = 0. \tag{9}$$

Now, $d = 0$ is identical to the enthalpy balance of a single first-order exothermic reaction with activation energy of $n\gamma \equiv E_a/RT$. In similarity to that problem $d = 0$ is single valued when $n\gamma < 4$ and multivalued other-

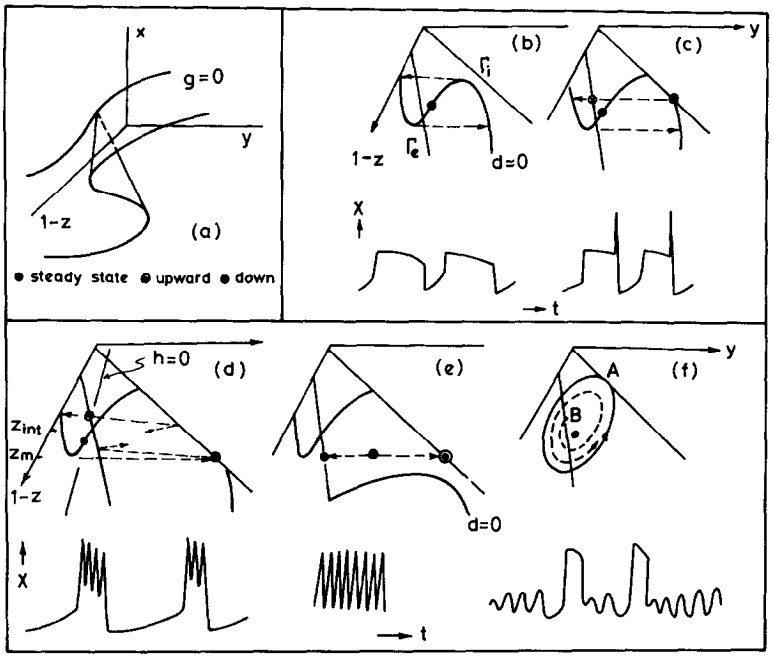

FIG. 5. Analysis of motion in a system of three widely separated time scales. The $g(x, y, z) = 0$ surface shown in (a) applies to all the situations shown; (b)–(f) present projections of motions on the $x = 0$ plane and time traces.

wise. Increasing the temperature (Y) leads to higher rates and lower x for positive γ (Fig. 4b). When $\gamma < 0$ $d = 0$ is an ascending curve and the only state on the unstable section of $g = 0$ are saddle points which cannot be surrounded by a limit cycle.

Heat transfer resistance may induce, therefore, oscillatory behavior in an autocatalytic kinetic scheme of two steps in series if the activation energy of the first (i.e., oxygen adsorption) is larger than that of the latter step (reaction) and if the heat capacity is sufficiently large. The limit cycle solution is composed then of slow sections separated by isothermal "jumps" in the reaction rate. Peaks in reaction rate precede those in temperature and temperature amplitude is independent of the heat transfer coefficient (Fig. 4). These characteristics are markedly different from those of thermokinetic oscillations which are dependent on transport properties and in which the reaction rate lags behind the temperature. Increasing the heat transfer coefficient should eventually eliminate the oscillation altogether ($T \to T_b$ as $h \to \infty$).

(c) *Complex Behavior (Fig. 5)*

We proceed with the analysis of the general third-order system (Eq. (6)), with wide separation of time scales. When heat capacity is large and surface oxidation is slow (τ_y, $\tau_z \gg \tau_x$) then

$$\frac{dy}{dx} = \frac{f}{g}\frac{\tau_x}{\tau_y} \to 0,$$

$$\frac{dz}{dx} = \frac{h}{g}\frac{\tau_x}{\tau_z} \to 0. \qquad (10)$$

Far from $g = 0$ the system moves fast in the direction of that surface and once on $g = 0$ the motion is governed by $dy/dt = f/\tau_y$, $dz/dt = h/\tau_z$. Writing $g = 0$ in form

$$\frac{Y}{(1-z)^2c^2}(1 - v - \beta v) = v(1-v)^2,$$

$$v = \frac{x}{1-x} \qquad (11)$$

we conclude from Fig. 4a that for any physical z and $8\beta < 1$ the $g = 0$ surface forms a multivalued manifold (Fig. 5a). The boundaries of the stable upper and lower folds are defined by the tangence of the straight line and the curve $v(1 - v)^2$ (Fig. 4a) at v_i, v_e. The ignition and extinction lines are dependent on β only. The projections of these lines (Γ_i, Γ_e in Fig. 5) are

$$Y = A_{i,e}[(1 - z)c]^2;$$
$$A_i = \frac{v_i(1 - v_i)}{1 - v_i - \beta v_i} \qquad (12)$$

with similar definition for A_e. To make the solution analytical we need to determine the motion on the stable folds of $g = 0$. That is possible if $\tau_y \ll \tau_z$: the motion is composed then of "jumps" in temperature (y) and slow motion along the subset of $f = 0$ which lies on $g = 0$. This line, the intersection of the two surfaces, satisfies

$$d(y, z) \equiv \frac{H}{1 - z} y - Y^n(1 - v - \beta v) = 0 \qquad (13)$$

with $v = v(y, z)$ along $g = 0$.

The hierarchy of time scales, $\tau_x \ll \tau_y \ll \tau_z$, allows for analytical solutions in the following cases, assuming the existence of a unique steady state:

(a) The projection of $d(y, z)$ from the lower fold onto the plane $x = 0$ is monotonic—the steady state is stable.

(b) The projection is multivalued and $d = 0$ does not intersect Γ_i (Fig. 5b)—the state is stable when it belongs to the stable sections of $d = 0$ and unstable when it lies on the intermediate branch. In the latter case the limit cycle is confined to the lower fold. The reaction rate amplitude is relatively small and the period is of $O(\tau_z)$.

(c) $d = 0$ intersects the ignition line (Fig. 5c)—the motion on the lower fold is still at $z = \text{const}$ with intermediate time scale (τ_y), followed by slow change along $d = 0$ until Γ_i is reached. Since the intermediate fold is not attracting, the system then moves fast vertically upward until the upper fold is reached. We now have to define the direction of motion on that fold. From Eq. (13) it is clear that the shape of $d = 0$ is retained on the upper fold, except that it is shifted to larger $(1 - z)$ values since v is larger (e.g., see Fig. 5e). That shift depends only on β and is usually large enough so that $d = 0$ is not intercepted on the upper fold. The motion then is to the left ($\dot{y} < 0$) at constant z until Γ_e is reached. The system moves back to the lower fold and resumes the usual course. The resulting time trace acquires a large reaction rate amplitude and it incorporates all three time scales, although it may be difficult to experimentally differentiate among the two fast scales.

(d) For the layout shown in Fig. 5d there exists a certain domain (z_m, z_{int}) where the motion on the upper and the lower folds does not intercept $d = 0$. This motion, which is at opposite directions on the two folds, may form a closed cycle only when $h(x, y, z)$ changed sign along the cycle. If $h > 0$ on both folds, then the approximation $z = \text{const}$ does not hold and the system will alternate between the upper and lower folds with $(1 - z)$ declining slowly, at a rate that depends on the ratio τ_y/τ_z. That requires the definition of the $h = 0$ equation and its intersection with $g = 0$ on both folds. For the sake of comprehension let us assume that $h = 0$ is a plane perpendicular to $x = 0$ and the projection of its intercept with $g = 0$ is a straight line passing, of course, through the steady state. For the situation shown in Fig. 5d, where the steady state is located outside the region of overlapping folds, $h > 0$ in $z_{int} < z < z_m$. The alternating-folds motion will continue until its interception with $d = 0$ at around z_{int}. At that point, where $d = 0$ intersects Γ_e, the system is drawn to the stable branch of $d = 0$. From there on it moves slowly to z_m to start a new cycle. The resulting multipeak cycle resembles superposition of a high-frequency train of cycles on a slow periodic behavior. Analytical solution to the number of peaks is not possible in this case, and that number may vary by one from one train to another.

If the alternating-folds motion intercepts $h = 0$ it may settle into a short-period (of order τ_y) cycle. This is the situation when a unique state exists on the intermediate unstable fold of $g = 0$ (Fig. 5e). It may also occur when the steady state is on the lower fold but actual integration is required to verify its existence.

We will avoid here the proof that the curve $d = 0$ may indeed acquire the multivalued shape, and cross the ignition or extinction lines or both. Note that the outlays shown in Figs. 5b–c can be achieved by a perturbation from a set of parameters where $d = 0$ is multivalued and tangent to the ignition line. It can be shown that there exists such a set.

(*d*) *Source of Chaos*

The preceding discussion demonstrates that the coupling of two oscillators, that of adsorbed oxygen–temperature with the temperature–surface oxide one, can produce the respective individual time traces as well as superposition of the two. In none of the mechanisms discussed so far, can we claim that the system will settle into a truly aperiodic motion. Theoretical considerations suggest, however, that following the transition from simple one-peak cycles to multipeak cycles there may exist a transition to chaotic solutions. It may be easier to achieve such solutions if the demand for three widely separated time scales is relaxed. This demand prohibits large variations in the shape of cycle when it involves sections of slow motion. Such separation may be also difficult to achieve physically. Analyzing system (6) when the thermal and surface modification time scales are similar yet τ_z, $\tau_y \gg \tau_x$, requires integration of the motion on each fold. Consider the situation shown in Fig. 5f drawn for the same set of parameters as Fig. 5c: when τ_z/τ_y is sufficiently small the steady state is stable, while when it is large the trajectories escape the lower fold (Fig. 5c). At some $(\tau_z/\tau_y)^*$ the limit cycle (solid line) is tangent to Γ_i at A. At that point the trajectory shoots to the upper fold. Since there are no attracting points or cycles there, the trajectory will eventually return to the lower fold. Now, if the return point (B) occurs within the limit cycle, the following spiral motion (broken line) will approach again the limit cycle. This will take an infinite time for the situation shown; upon a further increase in τ_y, however, that sequence of events will occur at a finite time and will repeat itself. The resulting time trace is of a periodic multipeak or truly aperiodic nature.

(*e*) *Comparison with Observations*

Consider the time traces of O_2 outlet concentration observed by Kurtanjek (*29*) during Ni-catalyzed H_2 oxidation, in a CSTR-like reactor (Fig. 6). These traces were accompanied by measurements of surface potential and surface temperature oscillations which exhibited a 1–3°C amplitude. The trace at 1.2 vol% O_2 in feed resembles superposition of a high-frequency oscillations on a long-period cycle suggesting the existence of three time scales. The superimposed cycle almost vanish at 1 vol% O_2 in feed and at even lower concentrations the time trace resembles that of Fig. 5f.

COMMUNICATION AND SYNCHRONIZATION

(*a*) *Analysis of the Two-Cell Problem*

Consider the interaction problem of two identical, open, well-mixed cells (Fig. 7a): no concentration and temperature gradients exist within each cell and they exchange mass and enthalpy with their surroundings. The equation describing the autocatalytic species in cell 1 is

$$M_x \frac{dx_1}{dt} = k_x g(x_1, y_1) - k_e a_v (x_1 - x_2). \quad (14)$$

The intercell communication term is the product of an effective exchange coefficient (k_e), the exchange area per unit volume (a_v), and the concentration gradient. The sign of the latter is reversed in the balance on cell 2. Since k_e if of order $D_x M_x a_v$, where $1/a_v$ is an approximation for the size of the diffusion boundary layer, we can write the equa-

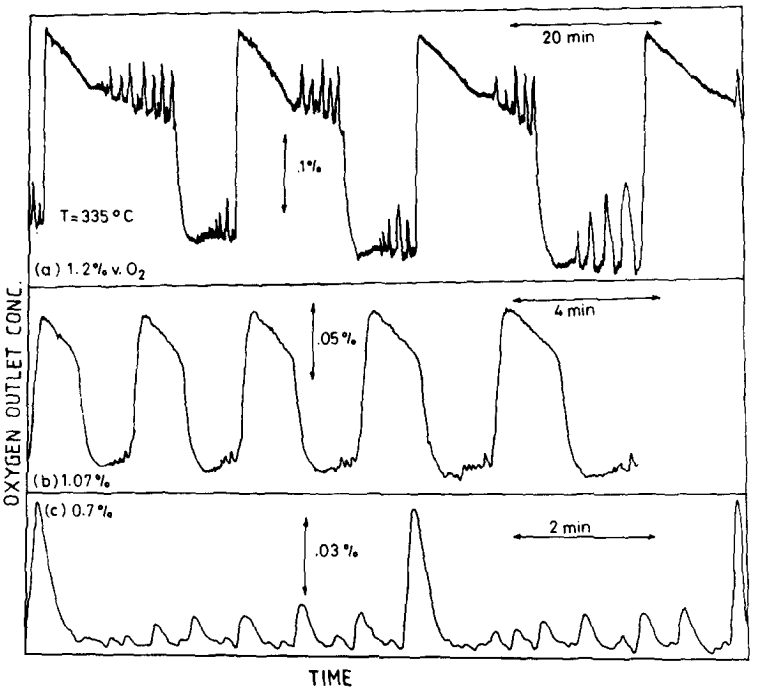

FIG. 6. Complex behavior observed by Kurtanjek (29) during H_2 oxidation on a Ni plate at three different inlet oxygen concentrations.

tions in the form

$$\tau_x \frac{dx_i}{dt} = g(x_i, y_i) \mp (L_x a_v)^2 (x_1 - x_2). \quad (15)$$

Similarly, for the nonautocatalytic variable we write

$$\tau_y \frac{dy_i}{dt} = f(x_i, y_i) \mp (L_y a_v)^2 (y_1 - y_2). \quad (16)$$

$L_i = (D_i M_k / k_i)^{1/2} = (D_i \tau_i)^{1/2}$ is the length scale associated with intercell exchange and it depends on the reaction velocity associated with the variable and the respective diffusivity.

The diffusivity varies significantly from one phase to another: it is of order 1 cm^2/s in the gas phase, 10^{-4}–10^{-6} cm^2/s in the adsorbed (i.e., two-dimensional liquid) phase, and it is estimated to be 10^{-10}–10^{-12} cm^2/s in the solid phase. The calculated length

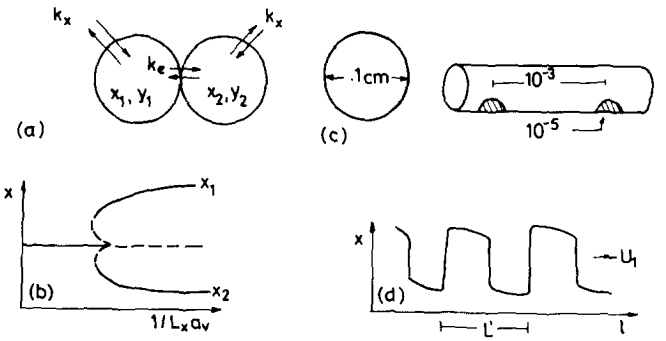

FIG. 7. Concepts in communication and synchronization. (a) The two-cell approach; (b) the emergence of asymmetric states with decreasing communication; (c) typical distances within a pellet and a pore; (d) synchronization in the form of a constant-velocity propagating wave.

scales (Table 2) are based on a typical oscillatory state with a period (i.e., τ_y) of 100 s and a turnover number (i.e., $1/\tau_x$) of 1 s^{-1}. The tabulated values clearly show that there usually exists a wide separation of length scales. Now, over distances (i.e., a_v^{-1}) much smaller than L_x and L_y the communication term (Eq. (15)) is strong enough to assure good synchronization, i.e., $x_1 = x_2$ and $y_1 = y_2$ at any time. For intermediate distances when the autocatalytic variable is long ranged, ($L_x \gg 1/a_v \gg L_y$) we conclude that $x_1 = x_2 = x$ while from Eq. (16) we demand that at steady state

$$(L_y a_v)^2(y_1 - y_2) = f(x_1, y_1) = -f(x_1, y_2). \quad (17)$$

Since $f(x, y) = 0$ is single valued, i.e., there exists a unique solution for any x, the above condition can be satisfied only at the uniform steady state ($y_1 = y_2$). Extension of the analysis to a string of cells, i.e., a continuous system, would lead to the same conclusion of uniqueness of the steady state. Analysis of the dynamic behavior would show that when the steady state is unstable, then uniform periodic behavior is the only solution in a two-cell system:

$$y_1(t) = y_2(t).$$

A long-ranged nonautocatalytic variable $L_y \gg 1/a_v$ assures that $y_1 = y_2 = y$. We write then an integral balance on y, and the system is modeled by

$$\tau_x \frac{dx_1}{dt} = g(x_1, y) - (L_x a_v)^2(x_1 - x_2)$$

$$\tau_x \frac{dx_2}{dt} = g(x_2, y) + (L_x a_v)^2(x_1 - x_2)$$

$$\tau_y \frac{dy}{dt} = \tfrac{1}{2} f(x_1, y) + \tfrac{1}{2} f(x_2, y). \quad (18)$$

At steady state we require that

$$(L_x a_v)^2(x_1 - x_2) = g(x_1, y) = -g(x_2, y). \quad (19)$$

When $g(x, y)$ is composed of two contributions (Fig. 4a), this condition lends itself to a simple graphical interpretation: x_1 and x_2 are located at positions which are equidistant between the two lines on opposite sides of the intermediate intersection point (x_0). The actual positions of x_1, x_2, and y are determined from the integral balance (Eq. (*18*)). The graphical construction shows that such an asymmetric solution exists only in the y domain that $g = 0$ is multivalued. As $L_x a_v \to 0$ the nonuniform solution is given by

$$g(x_{1\infty}, y_\infty) = g(x_{2\infty}, y_\infty) = f(x_{1\infty}, y_\infty) + f(x_{2\infty}, y_\infty) = 0. \quad (20)$$

With increasing degree of communication the concentration gradient ($x_1 - x_2$) diminishes. The asymmetry is eventually destroyed by coalescence with the uniform solution (Fig. 7b) which exists for any L_x. At that point the Jacobian matrix of (19) is singular, leading to the condition

$$2(L_x a_v)^2 = \left.\frac{\partial g}{\partial x}\right|_u \quad (21)$$

that should be satisfied at the uniform state. The stability analysis is somewhat more intricate but it shows that (a) the uniform state is always unstable, hence unobservable, beyond the bifurcation point (Fig. 7b) and that (b) the asymmetric states may be unstable when $L_x a_v$ and τ_x/τ_y are sufficiently small. In the latter case a limit cycle exists.

(*b*) *Physical Considerations*

Applying these arguments to the models under consideration (Table 2) we conclude that if the gas-phase concentration is the autocatalytic variable (Model I, $L_x \sim 1$ cm) it assures effective communication on the scale of a pellet or a plate as well as on smaller scales (Fig. 7c). When the gas-phase concentration is the nonautocatalytic variable (Model II) it may assumed to be well mixed but then synchronization is not assured even at the single crystallite level. These conditions will lead to symmetry breaking which may take on the following forms: an inhomogeneity within a single crystallite, a proportional distribution of crystallites in a supported catalyst between

states x_1 and x_2, or a certain spatial structure such as islands of oxidized surface in a polycrystalline surface. Reaction rate oscillations will not be observed in any of these cases. When both variables are surface concentrations and the autocatalytic one is long ranged (Models III, IV, $L_x \sim 10^{-3}$ cm) then effective synchronization is achieved over short distances. This situation poses two problems: (i) what is the intercrystallite communication mechanism in supported catalyst and (ii) is synchronization achieved across an unsupported catalytic surface? To answer the first question we have to consider diffusion through the support. Pismen (*15*) has analyzed the second problem to show that synchronization in the form of a constant velocity propagating wave (Fig. 7d) is achieved when $L' = L_x\tau_y/\tau_x \gg L_y$. Even though the periodic behavior persists locally in that situation, oscillations may go undetected if the wavelength, which is of order L' (0.1–1 cm), is much smaller than the catalyst size. Such behavior may account for the observations by Kurtanjek *et al.* (*7*) of a time-invariant bulk reaction rate while local oscillations of surface potential persist.

The discussion above suggest that a gas-phase autocatalytic variable (Model I) is necessary to assume efficient communication across a truly isothermal catalytic surface or pellet. We have concluded earlier, however, that the most likely two-variable model is the one that incorporates two surface concentrations (Model III). This necessitates the incorporation of mass and heat transfer resistances and the analysis of the resulting four (or five) variables model. Due to the long-range character of the gas-phase concentrations and the temperature, their incorporation may alter considerably the analysis even under conditions of small transport resistances.

We will not attempt to pursue here this analysis but mainly point out that the contribution of the long-range variables does not necessarily enhance the synchronization. Consider, for example, the nonisothermal model of Eq. (6). If $E_r < E_a$ then surface concentration is the short-ranged autocatalytic variable while temperature is long ranged. These conditions will induce inhomogeneities of one of the forms that were already discussed. When $E_r > E_a$ the nonisothermal model admits uniform unique or multiple solutions but cannot account for inhomogeneity in time (oscillations) or space. If that model is coupled now with a slow surface modification (Eq. (6)) it will predict homogeneous oscillations due to fast thermal communication.

(*c*) *Structure Sensitivity Induced by Asymmetry*

Due to the highly nonlinear kinetics the average rate of an asymmetric surface state may differ significantly from that of the uniform one. The emergence of inhomogeneous states induces dependence of the specific reaction rate (i.e., average turnover number) on a geometrical factor. This suggests a possible relation to the phenomena of structure sensitivity if the effective range for symmetry breaking is that of a crystalline size. To achieve such short range we may assume surface oxide to be the autocatalytic variable ($L_x \sim 100$ Å) while the nonautocatalytic variable is long ranged. The latter requirement is easily fulfilled even when the slow variable is a surface concentration ($L_y \sim 10^{-2}$ cm, Model V).

The crystallite is modeled as a one-dimensional system with zero-flux boundary conditions at its edges. The mathematical formulation of Model V at steady state, takes the form

$$g(x, y) + L_x^2 \frac{d^2x}{dl^2} = 0;$$

$$\frac{dx}{dl}(0) = \frac{dx}{dl}(L) = 0;$$

$$f(x, y) = \gamma c(1 - \bar{x} - y) - y = 0. \quad (22)$$

The autocatalytic function $g(x, y)$ is specified in Table 2 with the dimensionless fuel gas-phase concentration as a parameter (c).

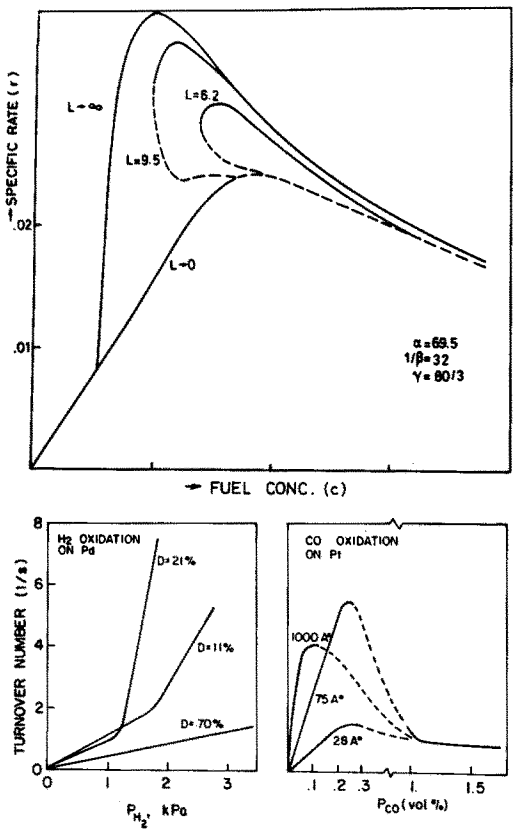

FIG. 8. Simulation and observations of structure sensitivity.

It accounts for surface oxidation and reduction. Surface modification is assumed to be slow reversible adsorption of F that forms inactive sites. That interpretation allows for increasing inhibition as c increases (f in Eq. (22)). Since $L_y \gg 1/a_v$ we may assume that y is space invariant and write an integral equation ($\bar{x}$ is space average).

The dependence of the dimensionless average rate on c is shown in Fig. 8a. With short crystallites the uniform rate curve exhibits a shallow maximum. When the crystallites are very large ($L \to \infty$) the branch of asymmetric states bifurcates from the uniform one at some c_b, and exhibits a much sharper maximum. The location and magnitude of the maximal rate varies with length. At large fuel concentrations the size dependence is much weaker or disappears altogether.

(d) Comparison with Observations

The similarity to the observations made by McCarthy *et al.* (*1*) during the study of Pt-catalyzed CO oxidation (Fig. 8b) is apparent: with increasing crystallite size the maximal rate is larger and it is shifted to lower concentrations. A distinct bifurcation point does not exist in this case; at large concentrations the rate is structure insensitive. Other investigators have observed size dependence in the region of negative-order kinetics. The data of Boudart *et al.* (*20*) suggests the existence of a bifurcation point in the rate curve of H_2 oxidation catalyzed by low-dispersion (large crystallite) palladium (Fig. 8c).

HETEROGENEOUS–HOMOGENEOUS MECHANISM (TABLE 3)

Consider a porous catalyst pellet where a homogeneous propagation reaction takes place in the pore volume, following a heterogeneous initiation reaction that forms intermediates (I) at the active catalyst of area A_v per unit pellet volume. Formal kinetic steps are presented in Table 3; for the sake of simplicity we assume that initiation is linear and that the net gain of I in the initiation and propagation step is identical. Termination can occur in the pore volume or heterogeneously on the support which has specific surface area S_g. There may exist a step of direct heterogeneous reaction (step 1).

We assume that the intercrystallites distance is sufficiently small so that all of these steps may be considered simultaneously. We also neglect pore diffusion resistance so that C and I concentrations are uniform within the pellet. The ordinary differential equations that model the system accounts for the kinetics and film mass transfer resistance. Let us assume further that loss of intermediate by transport is negligible. Redefining then the variables and the parameters we obtain a system of the form of Eq. (1). $g = 0$ implies

$$r(x) = x^2 + \gamma \frac{x}{1+x} = (\alpha + x)c \quad (23)$$

TABLE 3

Heterogeneous–Homogeneous Mechanism

Kinetic steps

(1) $F + O_2 \rightarrow B_1$	Surface reaction	$r_1 = k_1 C A_v$
(2) $F + O_2 \rightarrow \nu I + B_2$	Surface initiation	$r_2 = k_2 C A_v$
(3) $F + I + O_2 \rightarrow (1 + \nu)I + B_2$	Propagation	$r_3 = k_3 C I$
(4) $2I \rightarrow B_3$	Homogeneous termination	$r_4 = k_4 I^2$
(5) $I \rightarrow \frac{1}{2}B_3$	Heterogeneous termination	$r_5 = k_5 \dfrac{I}{1 + KI} S_g$

Equation

$$\frac{dC}{dt} = k_c S_x (C_b - C) - A_v(k_1 + k_2)C_1 - k_3 C I$$

$$\frac{dI}{dt} = \nu A_v k_1 C + \nu k_3 C I - k_4 I^2 - k_5 \frac{I}{1 + KI} - k_{cl} S_x I$$

Definitions

$$x = KI, \qquad c = \frac{\nu k_3 K}{k_4} C,$$

$$\tau_x = \frac{K}{k_4}, \ \tau_y = \frac{K}{k_3}, \ \alpha = \frac{K A_v k_2}{k_3}, \ \beta = \frac{k_3}{k_c a_v K}, \ \gamma = \frac{K k_5 S_g}{k_4}$$

Dimensionless equations

$$\tau_x \frac{dx}{dt} = \alpha c + cx - x^2 - \gamma \frac{x}{1 + x} \equiv g(x, c)$$

$$\tau_c \frac{dc}{dt} = \frac{c_b - c}{\beta} - \alpha \left(1 + \frac{k_1}{k_2}\right) c - xc \equiv f(x, c)$$

and may be solved graphically (Fig. 9a) by varying the slope of the straight line (c). The solution is unique for any c if the intercept of the line ($-\alpha$) is located sufficiently far from the origin, i.e., if the rate of initiation is large. When

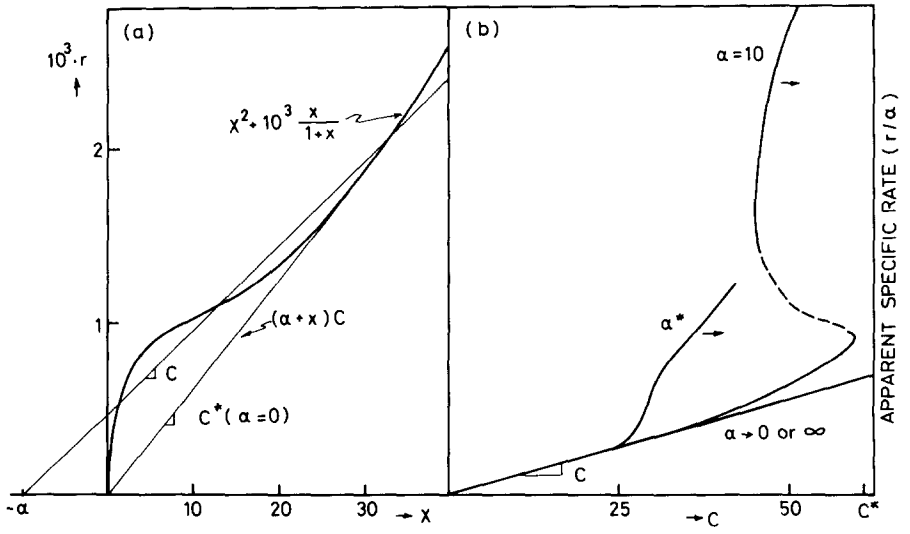

FIG. 9. Analysis of a heterogeneous–homogeneous mechanism. (a) Construction of steady-state solutions; and (b) apparent structure sensitivity upon varying active area (sintering).

$$\alpha \leq \alpha^* = \frac{(\gamma^{1/3} - 1)^3}{3\gamma^{1/3} - 2} \qquad (24)$$

then $g(x, c) = 0$ is multivalued for some range of c (as in Fig. 2b, $c = y$). Thus, the intermediate concentration is the autocatalytic variable. The parameters of $f(x, c)$ can now be adjusted to produce a periodic solution when the termination velocity is sufficiently large compared with the propagation step (i.e., small τ_x/τ_c).

A common practice in studying structure sensitivity is to induce sintering that results in larger crystallites and smaller A_v (*1*). If the contribution of the homogeneous reaction is significant then the specific rate varies with A_v. To simulate that behavior we plot the specific rate dependence on the fuel concentration at steady state. Since A_v appears only in α, the ratio of initiation to propagation rate constants, then the specific rate is proportional to r/α with r given by Eq. (23), and $k_1 = 0$. The homogeneous reaction cannot sustain itself, without heterogeneous initiation ($\alpha = 0$), at concentrations below c^* (Fig. 9). Even at $c > c^*$ the state of nil reaction rate still exists unless the system is subjected to a large enough perturbation that drives it to the upper state. Thus, standard experiment of the catalytic effect of the support may not reveal the heterogeneous–homogeneous effects. For small catalyst loading ($\alpha \to 0$) the system exhibits steady-state multiplicity and the lower branch obeys $r/\alpha = c$. This is the low-concentration asymptote for any α since the contribution of the propagation step is small. With increasing α the ignition point occurs at low concentrations, and at $\alpha = \alpha^*$ the hysteresis loop disappears altogether. At very heavy loading ($\alpha \to \infty$) the intermediate concentration is large and so is the termination rate ($k_4 I^2$); the resulting specific rate curve is the linear initiation rate.

We should point out that steady-state multiplicity is not essential for the observation of apparent structure sensitivity. The multiplicity disappears upon elimination of step 5 but the specific rate dependence persists. The model also accounts for support effects since the heterogeneous termination rate depends on the nature of the support.

CONCLUSIONS

The mechanism of surface oxidation and reduction is now probably the best supported model to account for the periodic behavior in reactions catalyzed by transition (including noble) metals. This mechanism, which includes a slow surface modification, accounts also for observations of slow-transients, deactivation processes, or sluggish behavior that are common in catalytic oxidation reactions. Recent work suggests that supported and highly dispersed noble-metal crystallites are more susceptible to oxidation than large ones. The dispersed catalyst (<50 Å) can undergo complete oxidation at low temperatures and the rate of the subsequent reduction follows an autocatalytic pattern (*30*). These observations agree with our interpretation of structure sensitivity but may be accounted for by other models as well, such as one that includes rate dependence on size in the form of a Kelvin law. In any case, these observations support the kinetic interpretation of structure sensitivity. The subject of oxidation of unsupported catalysts is still controversial. Unsupported catalysts (wires, foils) are usually subjected to chemical or thermal etching before employing them in kinetic studies. This process of rearrangement results in a microstructure of fine particles or protrusions, which become smaller over a long period of time. Since small particles are more susceptible to oxidation that may explain the observations that an aged wire is more susceptible to show periodic behavior than a fresh one (*5*). Finally, surface rearrangement itself can be accounted for by the surface oxidation and reduction mechanism when symmetry breaking takes place. Consider an island of oxidized surface surrounded by reduced surface. Near the border the situation is like that in the two-cells situation

(Fig. 7a). The asymmetry in surface oxide concentration induces diffusion of metal oxide from the oxide-rich to the oxide-poor cell. Subsequent reduction in the latter and deposition of the metal leads to surface rearrangement (*19*).

It is not clear yet whether oscillations in oxidation reactions (Fig. 1) have common origin. A large number of formal mechanisms have been suggested in the literature. This line of investigation would not reveal the source of the periodic behavior, but only elucidate the kinetic features once the chemical origin is known. A reliable model of the phenomena would probably have to account for at least three dynamic variables—two surface concentrations coupled with surface temperature and/or a boundary layer concentration. The latter two may not be crucial in order to account for the oscillations, but are important to assure good synchronization.

One rapid source of communication, which was ignored in our discussion, is the electronic one. Asymmetry in concentrations induces a gradient of surface potential. Yet the mechanism of potential equalization and its effect on reaction rate are ill defined in such a system. This mechanism will still be lacking in supported catalysis.

Two nonconventional mechanisms, based on nonlinear kinetics, were suggested here for structure sensitivity. Another plausible mechanism is that of a size-dependent temperature of crystallites when their temperature differs from that of the support. The last hypothesis was employed by Jensen and Ray (*31*) to account for oscillatory behavior. Critical tests for this approach require the portrayal of rate curve dependence on crystallite size, catalyst loading, and support structure and nature. Very few accounts of this sort are given in the literature; most of the studies consider the dependence of these factors on the rate at specified conditions.

ACKNOWLEDGMENT

This work was supported by the U.S.–Israel Binational Science Foundation.

REFERENCES

1. McCarthy, E., Zahradnik, J., Kuczynski, G. C., and Carberry, J. J., *J. Catal.* **39,** 29 (1975).
2. Zuniga, J. E., and Luss, D., *J. Catal.* **53,** 312 (1978).
3. Flytzania-Stephanopoulos, M., Schmidt, L. D., and Caretta, R., *J. Catal.* **64,** 346 (1980).
4. Vayenas, C. G., Lee, B., and Michaels, J., *J. Catal.* **66,** 36 (1980).
5. Sheintuch, M., and Luss, D., *J. Catal.* **68,** 245 (1981).
6. Turner, J. E., Sales, B. C., and Maple, M. B., *Surf. Sci.* **103,** 54 (1981); **109,** 591 (1981).
7. Kurtanejek, Z., Sheintuch, M., and Luss, D., *J. Catal.* **66,** 11 (1980).
8. Inui, T., and Mitsuhashi, K., *Nippon Kagaku Kaishi* **9,** 1311 (1977).
9. Vayenas, C. G., and Michaels, J. N., *Surf. Sci.* **120,** L405 (1982).
10. Sales, B. C., Turner, J. E., and Maple, M. B., *Surf. Sci.* **112,** 272 (1981); **114,** 381 (1982).
11. Riekert, L., *Ber. Bunsenges. Phys. Chem.* **85,** 297 (1981).
12. Varghese, P., Carberry, J. J., and Wolf, E. E., *J. Catal.* **55,** 76 (1978).
13. Schmitz, R. A., Renola, G. T., and Zioudas, A. P., *in* "Dynamics and Modelling of Reactive Systems" (W. E. Stewart, W. H. Ray, and C. C. Conley, Eds.), pp. 172–193. Academic Press, New York, 1980.
14. Chang, H. C., and Aluko, M., *Chem. Eng. Sci.* **36,** 1611 (1981).
15. Pismen, L. M., *Chem. Eng. Sci.* **35,** 1950 (1980).
16. Sheintuch, M., and Pismen, L. M., *Chem. Eng. Sci.* **36,** 489 (1981).
17. Prigogine, I., and Lefever, R., *J. Chem. Phys.* **48,** 1695 (1968).
18. Pismen, L. M., *Chem. Eng. Sci.* **34,** 563 (1979).
19. Sheintuch, M., *Chem. Eng. Sci.* **36,** 893 (1981); **37,** 591 (1982).
20. Boudart, M., Hanson, F. V., and Beagle, B., Paper presented at the 69th AIChE Meeting, Chicago, Nov. 1976.
21. Trimm, D. L., Corrie, J., and Lam, W., *J. Catal.* **60,** 476 (1979).
22. Ostapiuk, V. A., Boldireva, N. A., and Kozneichuk, G. K., *React. Kinet. Catal. Lett.* **16,** 151 (1981).
23. Bakaev, I. I., Aseev, I. V., Koshnaykov, A. M., and Novachenko, E. B., *Zh. Fiz. Khim.* **49,** 1719 (1975).
24. Berman, A. D., and Elinek, A. V., *Dokl. Akad. Nauk SSSR* **248,** 643 (1979).
25. Sheintuch, M., and Schmitz, R. A., *Catal. Rev. Sci. Eng.* **15,** 107 (1977).
26. Nicolis, G., and Prigogine, I., "Self Organization

in Nonequilibrium Systems." Wiley, New York, 1979.
27. Eigenberger, G., *Chem. Eng. Sci.* **33,** 1255; **33,** 1263 (1978).
28. Ertl, G., Norton, P. R., and Rustig, J., *Phys. Rev. Lett.* **49,** 177 (1982).
29. Kurtanjek, Z., Ph.D. dissertation. University of Houston, 1980.
30. Herz, R. K., and Shinouskis, E. J., *Appl. Surf. Sci.*, in press.
31. Jensen, K. F., and Ray, W. H., *Chem. Eng. Sci.* **35,** 2415 (1980); **35,** 2439 (1980).